STRESS DISTRIBUTIONS IN THIN-WALLED INTERSECTING CYLINDRICAL SHELLS SUBJECTED TO INTERNAL PRESSURE AND IN-PLANE FORCE

Y. ANDO, G. YAGAWA, F. KIKUCHI,

Department of Nuclear Engineering, The Faculty of Engineering, University of Tokyo, Tokyo, Japan

ABSTRACT

Stress analysis has been made with the application of the finite element method for the cases where the branch and the main pipes with nearly equal radii intersect at the angle of not only 90° but also 60° and 30°. Here, the considered loads are the internal pressure or the in-plane force applied at the end of the branch pipe. The Hellinger-Reissner's variational functional was derived for the Novozhilov's and Mushtari-Vlasov shell theory. Further, considering the curvature as infinity in case of the above mentioned theories the element matrix was determined for the flat plate element which was derived by Herrmann.

Comparison was made between the computed values and the results of the experiment which was carried out for steel models.

1. INTRODUCTION

Branch pipe is often used in the piping system of nuclear plant. Quite a good number of theoretical and experimental investigations were made on the stress distribution of pressure vessels with nozzles subjected to internal pressure or external load. These investigations are summarized in the book of reference [1].

It is important to estimate the magnitude of stress concentration at the branch pipe attachment when designing the piping structures for nuclear plant. As for the radial nozzle-to-shell attachment a few examples of analytical approach exist [2], [3], where the diameter of the nozzle pipe is much smaller than that of the cylinder. In case of the actual piping system where the nozzle pipe and the cylinder have nearly identical diameters the application of the above theories becomes difficult because of the convergence problem of the solution. And the analytical methods applied so far bring complexity in the analysis of nonradial nozzle-to-shell attachments. The application of the finite element method can, however, solve all these problems.

This paper reports an investigation on the analytical calculation with the finite element method and the measurement of stress distribution for the branch pipe subjected

to internal pressure or in-plane force where the nozzle pipe & the cylinder possess nearly identical diameters and the intersecting angle is 90° or less. At first the finite element method with the mixed model element of Herrmann et al.[4],[5] was modified to the Novozhilov & Donnell type for general shell. This method showed superiority over the compatible model element method because of the simple expression of the characteristic matrix and a very short time of computation. The accuracy of a few theories was evaluated for some simple cases. Triangular flat element was used in the analysis, and quite good correlation between the experimental and the computed values was obtained.

2. THEORY OF THE FINITE ELEMENT METHOD

Let the curvilinear orthogonal coordinates (α, β) represent the principal directions of curvature at the mid-plane of a shell shown in fig. 1. Let the radii of curvature be R_α & R_β corresponding to the axes α & β respectively. Let the Z-axis be the normal direction to the mid-plane of the shell, and the displacement in the α, β & Z directions be represented by u, v & w respectively. The strain-displacement relation is given by Novozhilov [6] as follows:

$$
\left.
\begin{aligned}
\varepsilon_\alpha &= \frac{1}{A}\frac{\partial u}{\partial \alpha} + \frac{v}{AB}\frac{\partial A}{\partial \beta} - \frac{w}{R_\alpha} \\
\varepsilon_\beta &= \frac{1}{B}\frac{\partial v}{\partial \beta} + \frac{u}{AB}\frac{\partial B}{\partial \alpha} - \frac{w}{R_\beta} \\
\gamma_{\alpha\beta} &= \frac{1}{B}\frac{\partial u}{\partial \beta} - \frac{v}{AB}\frac{\partial B}{\partial \alpha} + \frac{1}{A}\frac{\partial v}{\partial \alpha} - \frac{u}{AB}\frac{\partial A}{\partial \beta} \\
K_\alpha &= \frac{1}{A}\frac{\partial}{\partial \alpha}\left(\frac{1}{A}\frac{\partial w}{\partial \alpha}\right) + \frac{1}{AB^2}\frac{\partial A}{\partial \beta}\frac{\partial w}{\partial \beta} + \frac{1}{A}\frac{\partial}{\partial \alpha}\left(\frac{u}{R_\alpha}\right) + \frac{1}{AB}\frac{v}{R_\beta}\frac{\partial A}{\partial \beta} \\
K_\beta &= \frac{1}{B}\frac{\partial}{\partial \beta}\left(\frac{1}{B}\frac{\partial w}{\partial \beta}\right) + \frac{1}{A^2B}\frac{\partial B}{\partial \alpha}\frac{\partial w}{\partial \alpha} + \frac{1}{B}\frac{\partial}{\partial \beta}\left(\frac{v}{R_\beta}\right) + \frac{1}{AB}\frac{u}{R_\alpha}\frac{\partial B}{\partial \alpha} \\
K_{\alpha\beta} &= \frac{1}{AB}\left(\frac{\partial^2 w}{\partial \alpha \partial \beta} - \frac{1}{A}\frac{\partial A}{\partial \beta}\frac{\partial w}{\partial \alpha} - \frac{1}{B}\frac{\partial B}{\partial \alpha}\frac{\partial w}{\partial \beta}\right) + \frac{1}{R_\alpha}\left(\frac{1}{B}\frac{\partial u}{\partial \beta} - \frac{u}{AB}\frac{\partial A}{\partial \beta}\right) + \frac{1}{R_\beta}\left(\frac{1}{A}\frac{\partial v}{\partial \alpha} - \frac{v}{AB}\frac{\partial B}{\partial \alpha}\right)
\end{aligned}
\right\} \quad (1)
$$

where A & B are Lamé's parameters.

The stress-strain relationship is expressed by the following equation (see fig. 2) :

$$
\left.
\begin{aligned}
&N_\alpha = \frac{Et}{1-\nu^2}(\varepsilon_\alpha + \nu\varepsilon_\beta) \quad , \quad N_\beta = \frac{Et}{1-\nu^2}(\varepsilon_\beta + \nu\varepsilon_\alpha) \\
&N_{\alpha\beta} = Gt\,\gamma_{\alpha\beta} - M_{\alpha\beta}/R_\beta \quad , \quad N_{\beta\alpha} = Gt\,\gamma_{\alpha\beta} - M_{\beta\alpha}/R_\alpha \\
&M_\alpha = -D(K_\alpha + \nu K_\beta), \; M_\beta = -D(K_\beta + \nu K_\alpha), \; M_{\alpha\beta} = M_{\beta\alpha} = -D(1-\nu)\,\gamma_{\alpha\beta}
\end{aligned}
\right\} \quad (2)
$$

where E : Young's modulus

ν : Poisson's ratio (=0.3)

t : Wall thickness of the shell

$$G = \frac{E}{2(1+\nu)}$$

$$D = \frac{E\,t^3}{12(1-\nu^2)}$$

The following relationship exists between the shearing force and the bending moment :

$$
\left.
\begin{aligned}
AB\,Q_\alpha &= \frac{\partial}{\partial \alpha}(BM_\alpha) + \frac{\partial}{\partial \beta}(AM_{\beta\alpha}) + \frac{\partial A}{\partial \beta}M_{\alpha\beta} - \frac{\partial B}{\partial \alpha}M_\beta \\
AB\,Q_\beta &= \frac{\partial}{\partial \beta}(AM_\beta) + \frac{\partial}{\partial \alpha}(BM_{\alpha\beta}) + \frac{\partial B}{\partial \alpha}M_{\beta\alpha} - \frac{\partial A}{\partial \beta}M_\alpha
\end{aligned}
\right\} \quad (3)
$$

The equation of equilibrium is expressed as follows:

$$\left.\begin{aligned}
&\frac{\partial}{\partial\alpha}(BN_\alpha)+\frac{\partial}{\partial\beta}(AN_{\beta\alpha})+\frac{\partial A}{\partial\beta}N_{\alpha\beta}-\frac{\partial B}{\partial\alpha}N_\beta-\frac{AB}{R_\alpha}Q_\alpha+XAB=0\\
&\frac{\partial}{\partial\beta}(AN_\beta)+\frac{\partial}{\partial\alpha}(BN_{\alpha\beta})+\frac{\partial B}{\partial\alpha}N_{\beta\alpha}-\frac{\partial A}{\partial\beta}N_\alpha-\frac{AB}{R_\beta}Q_\beta+YAB=0\\
&\frac{\partial}{\partial\alpha}(BQ_\alpha)+\frac{\partial}{\partial\beta}(AQ_\beta)+AB\left(\frac{N_\alpha}{R_\alpha}+\frac{N_\beta}{R_\beta}\right)+pAB=0
\end{aligned}\right\} \qquad (4)$$

where X, Y and p represent distributed load for unit area in α, β and Z directions respectively at the mid-plane of the shell (see fig. 1)

Let the following equation represent the boundary conditions :

$$\left.\begin{aligned}
&u=\bar{u},\ v=\bar{v},\ w=\bar{w},\ \frac{\partial w}{\partial n}=\overline{\frac{\partial w}{\partial n}} && \text{on } C_1\\
&N_{sn}-\frac{M_{sn}}{R_s}=\overline{N_{sn}}-\overline{\frac{M_{sn}}{R_s}},\ N_{\beta n}-\frac{M_{\beta n}}{R_\beta}=\overline{N_{\beta n}}-\overline{\frac{M_{\beta n}}{R_\beta}},\ Q_n+\frac{\partial M_{ns}}{\partial s}=\overline{Q_n}+\overline{\frac{\partial M_{ns}}{\partial s}},\ M_n=\overline{M_n} && \text{on } C_2
\end{aligned}\right\} \qquad (5)$$

where the notation with bar represents the prescribed value at the boundary.

Now, let n & s be the outward normal direction and the tangential direction respectively at the boundary, and l & m be the direction cosines of the normal component as shown in fig. 3 . Then the following equation is valid:

$$\left.\begin{aligned}
&N_{sn}=N_s l+N_{\beta s}m,\ N_{\beta n}=N_{s\beta}l+N_\beta m\\
&M_n=M_s l^2+(M_{s\beta}+M_{\beta s})lm+M_\beta m^2,\ M_{ns}=(M_\beta-M_s)lm+M_{s\beta}l^2-M_{\beta s}m^2\\
&M_{sn}=M_s l+M_{\beta s}m,\ M_{\beta n}=M_{s\beta}l+M_\beta m,\ Q_n=Q_s l+Q_\beta m
\end{aligned}\right\} \qquad (6)$$

The equivalent variational functional Π in the above mentioned problem is given by the following equation:

$$\begin{aligned}
\Pi=\iint\Big\{&\frac{1}{2}\frac{Et}{1-\nu^2}\left[\varepsilon_s^2+\varepsilon_\beta^2+2\nu\varepsilon_s\varepsilon_\beta+\frac{1-\nu}{2}\gamma_{s\beta}^2\right]-(Xu+Yv+pw)\\
&-\frac{S}{2}\left[(M_s+M_\beta)^2+2(1+\nu)(M_{s\beta}^2-M_sM_\beta)\right]\\
&+\frac{1}{A^2B}\frac{\partial w}{\partial\alpha}\left[\frac{\partial(BM_s)}{\partial\alpha}+\frac{\partial(AM_{\beta s})}{\partial\beta}\right]+\frac{1}{AB^2}\frac{\partial w}{\partial\beta}\left[\frac{\partial(AM_\beta)}{\partial\beta}+\frac{\partial(BM_{s\beta})}{\partial\alpha}\right]\\
&-M_s\left[\frac{1}{AB^2}\frac{\partial A}{\partial\beta}\frac{\partial w}{\partial\beta}+\frac{1}{A}\frac{\partial}{\partial\alpha}\left(\frac{u}{R_s}\right)+\frac{1}{AB}\frac{v}{R_\beta}\frac{\partial A}{\partial\beta}\right]-M_\beta\left[\frac{1}{A^2B}\frac{\partial B}{\partial\alpha}\frac{\partial w}{\partial\alpha}+\frac{1}{B}\frac{\partial}{\partial\beta}\left(\frac{v}{R_\beta}\right)+\frac{1}{AB}\frac{u}{R_s}\frac{\partial B}{\partial\alpha}\right]\\
&+M_{s\beta}\left[\frac{1}{A^2B}\frac{\partial A}{\partial\beta}\frac{\partial w}{\partial\alpha}+\frac{1}{AB^2}\frac{\partial B}{\partial\alpha}\frac{\partial w}{\partial\beta}-\frac{2}{R_s}\left(\frac{1}{B}\frac{\partial u}{\partial\beta}-\frac{u}{AB}\frac{\partial A}{\partial\beta}\right)-\frac{2}{R_\beta}\left(\frac{1}{A}\frac{\partial v}{\partial\alpha}-\frac{v}{AB}\frac{\partial B}{\partial\alpha}\right)\right]\Big\}AB\,d\alpha d\beta\\
&-\oint_C M_{ns}\frac{\partial w}{\partial s}ds-\int_{C_1}M_n\overline{\frac{\partial w}{\partial n}}ds-\int_{C_2}\left[\left(\overline{N_{sn}}-\overline{\frac{M_{sn}}{R_s}}\right)u+\left(\overline{N_{\beta n}}-\overline{\frac{M_{\beta n}}{R_\beta}}\right)v+\left(\overline{Q_n}+\overline{\frac{\partial M_{ns}}{\partial s}}\right)w\right]ds
\end{aligned} \qquad (7)$$

where the independent functions are u, v, w, M_α, M_β and $M_{\alpha\beta}=M_{\beta\alpha}$ within the zone and u, v, w and $\partial w/\partial n$ at the boundary. The continuity of function between the elements is required for u, v, w and $\partial w/\partial n$. The basic boundary conditions are $u=\bar{u}$, $v=\bar{v}$, $w=\bar{w}$ and $N_n=\bar{N}_n$, and the rest are the natural boundary conditions. $\oint_C$ represents the integral for the all boundaries of elements, and $S=\frac{12}{Et^3}$.

In the above functional strain components ε_α, ε_β and $\gamma_{\alpha\beta}$ are calculated from eq. (1) .

To consider the curvilinear orthogonal coordinate on the mid-plane of a flat plate $\frac{1}{R_\alpha}=0$, $\frac{1}{R_\beta}=0$ are substituted in eq. (7). In the analysis of flat plate the part concerned with the membrane force can be completely separated from the part concerned with bending within the limit of the small displacement theory. The part concerned with

the membrane force totally coincides with the expression derived by the principle of minimum potential energy for plane stress problems.

In the theory of Mushtari-Vlasov [7] the terms for u & v in the curvature-displacement relation are omitted. Consequently, the terms for Q_α & Q_β in eq. (4) vanish, and the stress boundary conditions on C_σ become

$$N_{\alpha n} = \overline{N}_{\alpha n}\ ,\quad N_{\beta n} = \overline{N}_{\beta n}\ ,\quad Q_n + \frac{\partial M_{ns}}{\partial s} = \overline{Q}_n + \frac{\partial \overline{M}_{ns}}{\partial s}\ ,\quad M_n = \overline{M}_n \qquad (8)$$

Moreover, $N_{\alpha\beta} = N_{\beta\alpha} = Gt\,\gamma_{\alpha\beta}$. So, in eq.(7) the terms of u & v multiplied by the moment vanish for both area integral and line integral.

The general theory derived above was applied for the cylindrical shell and a few characteristic matrices were formed.

In a cylindrical shell let x-axis represent the longitudinal direction, y-axis represent the circumferential direction, z-axis represent the outward radial direction, and R be the radius. Then eq. (7) can be applied in this particular case substituting $\alpha = x$, $\beta = y$, $A = 1.0$, $B = 1.0$, $R_\alpha = \infty$, $R_\beta = -R$ in it. As for the characteristic matrix both rectangular and triangular elements were used, which are described below.

Three kinds of characteristic matrices were formed with the rectangular element which are

a) characteristic matrix of flat plate element

b) characteristic matrix of Novozhilov Type

c) characteristic matrix of Donnell Type

In either of the cases at the verteces 1,2,3,4 of the rectangle (see fig. 4) the values $(u_i,\ v_i,\ w_i)_{i=1,2,3,4}$ for u, v and w are given at the nodes, and at the sides 5,6,7,8 the values $(M_{ni})_{i=5,6,7,8}$ for M_n are given. Using the values at the verteces the expressions for u, v & w with in the element are given by

$$\left.\begin{aligned} u &= (1-\xi)(1-\eta)u_1 + \xi(1-\eta)u_2 + \xi\eta\, u_3 + (1-\xi)\eta\, u_4 \\ v &= (1-\xi)(1-\eta)v_1 + \xi(1-\eta)v_2 + \xi\eta\, v_3 + (1-\xi)\eta\, v_4 \\ w &= (1-\xi)(1-\eta)w_1 + \xi(1-\eta)w_2 + \xi\eta\, w_3 + (1-\xi)\eta\, w_4 \end{aligned}\right\} \qquad (9)$$

where

L_x : Distance on the x-axis of the rectangular element

L_y : Distance on the y-axis of the rectangular element

$0 \le x \le L_x$, $0 \le y \le L_y$

Now, let the distribution of the moment be obtained from the following equation:

$$M_x = \xi\, M_{n6} + (1-\xi)M_{n8}\ ,\quad M_y = (1-\eta)M_{n5} + \eta\, M_{n7} \qquad (10)$$

Here, M_{xy} is directly calculated from displacement. The distributions of displacement and moment as supposed above satisfy the desired continuity of the functions. If computation is executed using these distributions and eq. (7) the characteristic matrix is obtained easily.

Like the rectangular element three kinds of characteristic matrices can be derived for the triangular element also (see fig. 5). When the values $(u_i,\ v_i,\ w_i)_{i=1,2,3}$ of u, v & w at the three verteces $(x_i,\ y_i)_{i=1,2,3}$ of a triangle are known, the expressions

for u, v & w within the element are given by

$$u = \sum_{i=1}^{3} u_i \zeta_i \quad , \quad v = \sum_{i=1}^{3} v_i \zeta_i \quad , \quad w = \sum_{i=1}^{3} w_i \zeta_i \tag{11}$$

where

$$\left.\begin{aligned} &\zeta_i = A_i + B_i x + C_i y \ , \quad A_i = (x_2 y_3 - x_3 y_2)/2\Delta \ , \quad B_i = (y_2 - y_3)/2\Delta \\ &C_i = (x_3 - x_2)/2\Delta \ , \quad 2\Delta = x_1 y_3 - x_3 y_1 + x_3 y_1 - x_1 y_3 + x_1 y_2 - x_2 y_1 \end{aligned}\right\} \tag{12}$$

As for the moment the values $(M_{ni})_{i=4,5,6}$ of M_n on the three sides 4,5,6 of the triangle are given, and M_x, M_y& M_{xy} within the element are calculated from M_{ni}. So, the moment within the element is always constant.

3. CONVERGENCE OF THE FINITE ELEMENT SOLUTIONS

Let a line-loaded cylinder be considered as shown in fig. 6. Considering the symetry of the problem the length was divided into 1 element and the circumference was divided into n equal elements. Elements used were three kinds of rectangular elements. The convergence of the deflection w at the loading points is shown in fig. 7. It is clear from this figure that the value yielded by the flat plate element coincides fairly well with the exact solution for Novozhilov theory.

On one hand the convergence is poor in the case of Novozhilov type & Donnell type curved element. The convergence is not enough even for 100 divisions in this case.

The poorness of the convergence for the curved element is seemed to be due to the fact that the curved element does not include the rigid body mode in its displacement function.

4. CORRELATION BETWEEN ANALYTICAL AND EXPERIMENTAL STRESS DISTRIBUTIONS

Comparison will be made here between the computed values of the stress distribution and the experimental ones for steel model.

When internal pressure is applied to a radial nozzle-to-shell attachment as shown in fig. 8 the stress distributions are obtained as shown in figs. 9 & 10.

Fig. 9 shows the stress distribution on the outer surface of x-z plane of fig. 8. This is to be noted here that σ_n is the stress normall to the cross-section, and σ_t is the stress paralel to the cross-section. Fig. 10 shows the stress distributions σ_n & σ_t on y-z plane of fig. 8.

Next, considering the new axis z' (nozzle axis) on the x-z plane as shown in fig. 11 where θ is the angle between the x-axis and the z'-axis, let an in-plane force F be applied at the free end of the nozzle pipe. For the three intersecting angles of the nozzle-to-shell attachments as shown in the same figure the stress distributions are obtained as shown in figs. 12 to 14.

Fig. 12 shows the stress distribution at the outer surface of x-z' plane of radial nozzle-to-shell attachment (θ=90°). Figs. 13 & 14 show the stress distributions at the outer surfaces of the acute angle x-z' plane of nonradial nozzle-to-shell attachments for θ=60° & 30° respectively.

Quite good correlation is exhibited between the computed and the experimental values in case of the radial nozzle-to-shell attachment. But the correlation is not

so good in case of the nonradial nozzle-to-shell attachments. In the experimental models welding corner is round, but it is not considered in the computation. For the analysis of this part of the attachment it is thought necessary to apply the three dimensional finite element method.

This is to mention here that the computer time used for this calculation was 540 seconds by HITAC-5020 E and the order of the governing system of equations is about 2000 in the present problem.

5. CONCLUSION

This paper was described about the application of the Hellinger-Reissner's variational principle for the finite element method of general shell for the analysis of the arbitrary shell structure. As for the convergence it was verified that the convergence of the flat element is excellent in comparison with that of the curved one.

Stress analysis was conducted with the radial and nonradial nozzle-to-shell attachments, and reasonable evaluation was made on the correlation between the theoretical and the experimental values.

[REFERENCES]

[1] GILL, S.S., The stress analysis of pressure vessels and pressure vessel components, Pergamon Press (1970)

[2] ERINGEN, A.C., SUHUBI, E.S., "Stress distribution at two normally intersecting cylindrical shells", Nucl. Struct. Engr., Vol.2, 253 (1965)

[3] YAMAMOTO,Y., ET AL., "Theory of stress concentration of the normally intersecting cylindrical shells", Bulletin of JSME,Vol. 12, No. 49, 1(1969)

[4] HERRMANN, L.R., "Finite element bending analysis for plates", J. of the Engr. Mech. Div., Proc. of the ASCE, Vol.93, No.EM5, 13 (1967)

[5] HERRMANN, L.R., CAMPBELL, D.M., "A finite-element analysis for thin shells", AIAA J., Vol.6, No.10 1842 (1968)

[6] NOVOZHILOV, V.V., Thin shell theory, P.Noordhoff (1964)

[7] WASHIZU, K., Variational methods in elasticity and plasticity, Pergamon press (1968)

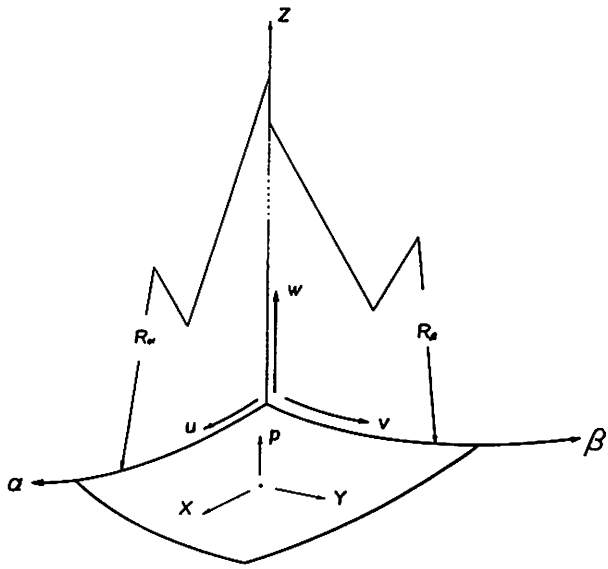

fig. 1 Coordinate system for a shell

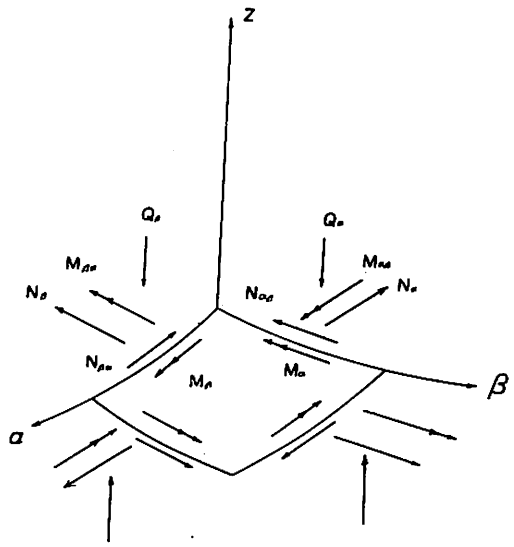

fig. 2 Nomenclature and sign conventions for stress resultants

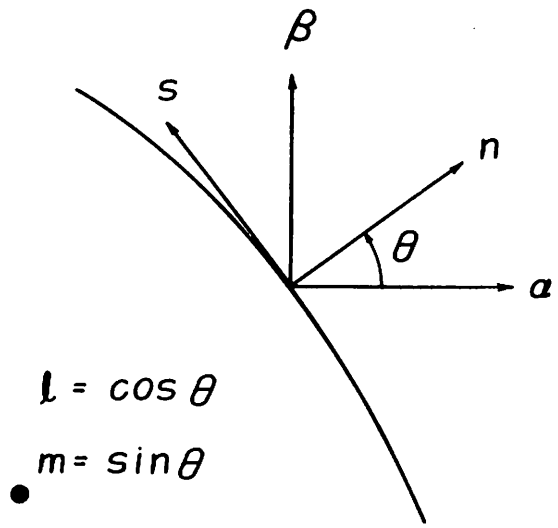

fig. 3 Geometrical relations on the boundary

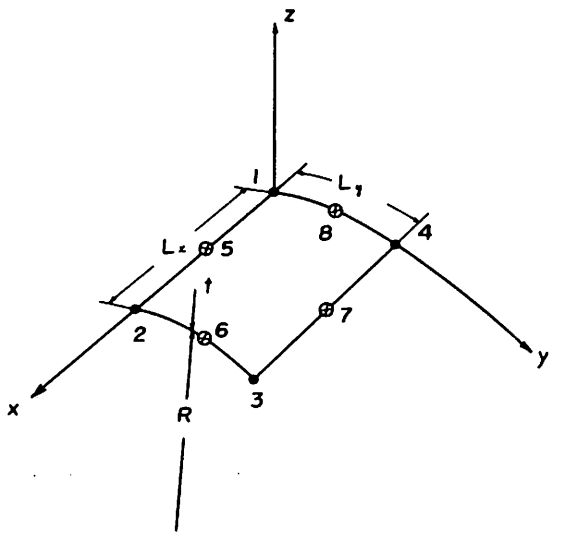

fig. 4 Rectangular element

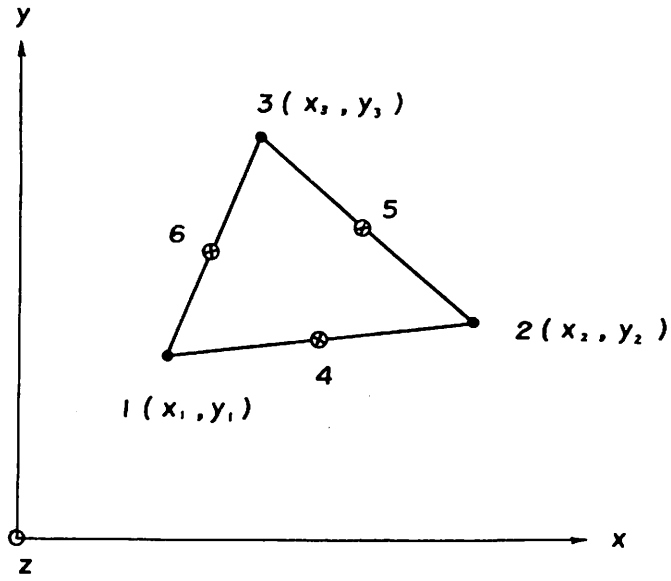

fig. 5 · Triangular element

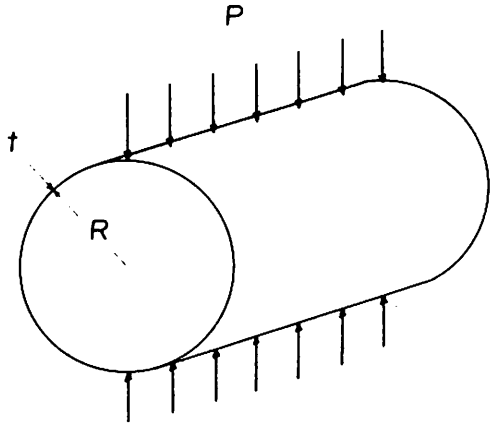

P = 1 lb/in.

R = 4.953 in.

E = 10.5 x 10^6 psi

t = 0.094 in.

ν = 0.3125

fig. 6 Infinite cylinder under line load

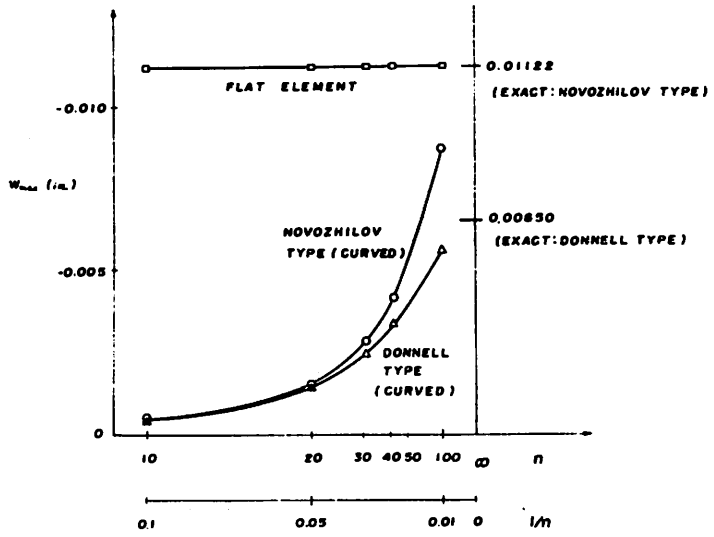

fig. 7 Convergence of the maximum deflection

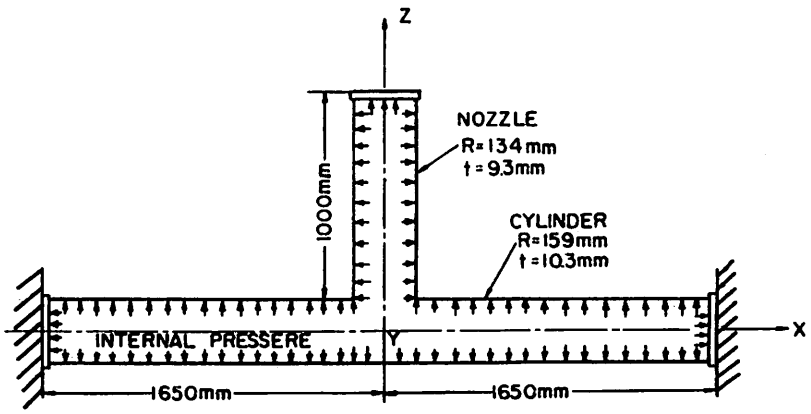

fig. 8 Nozzle-to-cylinder intersection under internal pressure p

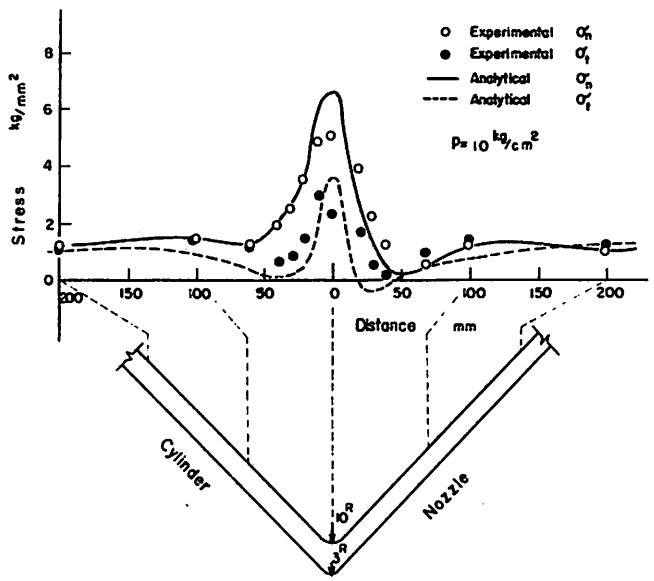

fig. 9 Experimental and analytical results on the longitudinal plane under 10 kg/cm² internal pressure

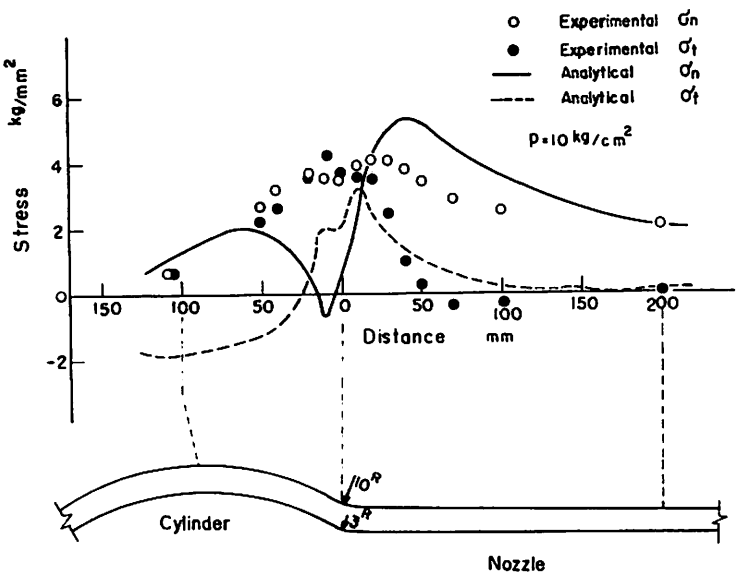

fig. 10 Experimental and analytical results on the transverse plane under 10 kg/cm² internal pressure

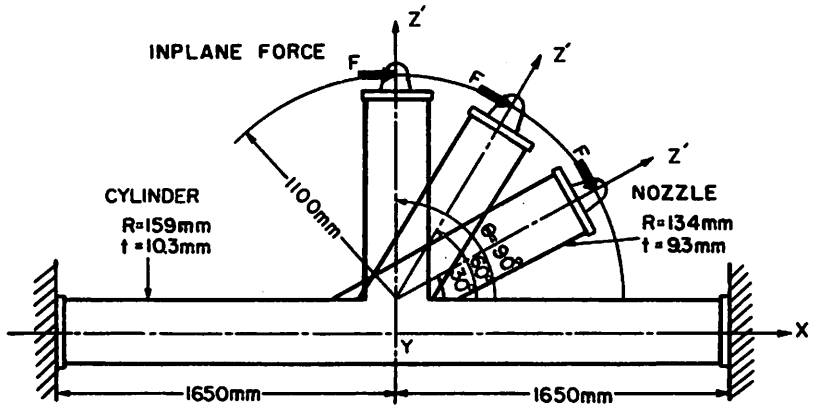

fig. 11 Nonradial nozzle-to-cylinder intersection under in-plane force F

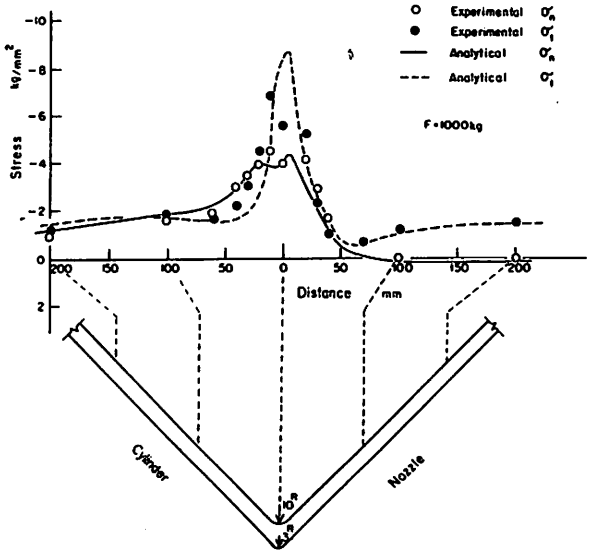

fig. 12 Experimental and analytical results on the longitudinal plane under 1000 kg in-plane force (θ=90°)

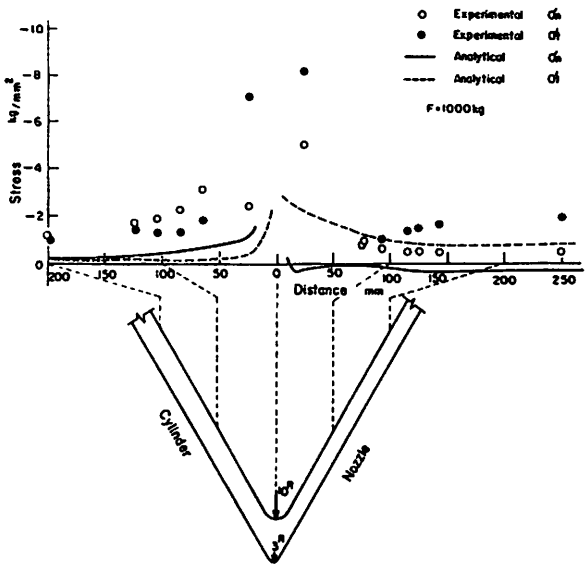

fig. 13 Experimental and analytical results on the longitudinal plane under 1000 kg in-plane force (θ =60°)

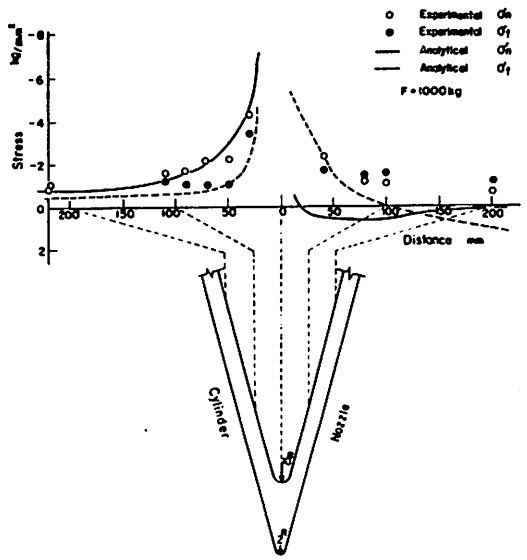

fig. 14 Experimental and analytical results on the longitudinal plane under 1000 kg in-plane force (θ =30°)

DISCUSSION

Q N. KRISHNAMURTHY, U. S. A.

For non-radial connections, your computed and measured results were shown on the slides as terminating on either side of the junction itself. But for the stress concentration phenomenon the maximum stress at the junction is important. How do you propose to obtain this value ?

A Y. ANDO, Japan

In this paper, we tried to get the most effective results within our financial limitation. But, if it is allowed, it should be better to measure the stress distribution of the inner surface of experimental models, especially at the region of intersection and to apply the three-dimensional finite element method in calculation.

Q E. GIENCKE, Germany

I believe, you get into difficulties because of the linear approximation for the stresses (normal forces, moments) as well as for the deformations in the finite elements. The order of the approximation for the deformations must be higher to get a better convergence of the results.

A Y. ANDO, Japan

We think that the poorness of convergence for the case of curved elements is mainly due to the fact that the rigid body mode in the displacement function is not included in the curved element, but we will examine this problem in detail.

A T. ARIMAN, U. S. A.

Although I am not very familiar with the use of the finite element method I would like to try for a possible answer to the question of Dr. Giencke. In the theoretical analysis of intersecting cylindrical shells the rigid body motions do not generate additional stresses. They appear as constants in the expressions of the displacement components. When you use the stress displacement relations due to the derivation they vanish.

A E. Y. W. TSUI, U. S. A.

Using similar curvilinear coordinates and including shear deformations, similar stiffness matrices for cylindrical and other finite elements have also been obtained recently by the discusser and his colleagues. Since the two-dimensional finite difference technique was used to obtain the resulting matrices, it appears to the discusser that rigid body modes for the elements of the stiffness matrices are not absolutely desirable, as far as their practical applicability is concerned.